Journal of Alloys and Compounds xxx (2013) xxx–xxx

Contents lists available at ScienceDirect

Journal of Alloys and Compounds

journal homepage: www.elsevier.com/locate/jalcom

Microstructural and mechanical characterizations of steel tubes joined by transient liquid phase bonding using an amorphous Fe–B–Si interlayer

Nicolas Di Luozzo [a,b,*], Béatrice Doisneau [b], Michel Boudard [b], Marcelo Fontana [a], Bibiana Arcondo [a]

[a] Laboratorio de Sólidos Amorfos, INTECIN, Facultad de Ingeniería, Universidad de Buenos Aires – CONICET, Paseo Colón 850, C1063ACV Buenos Aires, Argentina
[b] Laboratoire des Matériaux et du Génie Physique (CNRS UMR 5628), Grenoble Institute of Technology, MINATEC, Grenoble Cedex 1, France

ARTICLE INFO

Article history:
Available online xxxx

Keywords:
Transient liquid phase bonding process
Amorphous foil
Carbon steel
Electron backscattering diffraction
Mechanical properties

ABSTRACT

In this work the transient liquid phase bonding process was successfully used to join seamless carbon steel tubes using an amorphous Fe–B–Si foil as interlayer. The tubes were aligned with their butted surfaces in contact with the interlayer and the entire assembly was heated by means of an induction furnace under a reducing atmosphere. The temperature was raised to the process temperature (≈1300 °C) and then held for 7 min. The joining process was performed under a pressure of 5 MPa.

The joined tubes microstructures were characterized by direct observations – scanning electron microscopy – and diffraction techniques – electron backscatter diffraction. Chemical analysis was performed by electron probe microanalysis. The joint region (JR) presents only ferrite grains - in contrast with the heat affected zone (HAZ) and the base metal (BM), whose microstructures consist of ferrite and cementite. Si content at the JR was precisely determined by chemical profiling, showing higher concentrations of Si compared with the HAZ and BM. These results are in accordance with the fact that the cementite is unable to form in Si enriched zones. Also, ferrite grains at the JR present high-angle grain boundaries with respect to the grains of the HAZ.

Tensile tests show that the joined tubes failed away from the bond, at the HAZ, and reached 96% of the ultimate tensile strength of the BM, in the as-bonded condition. Microindentation hardness profiles across the bonding zone are in agreement with the observed microstructures at the different zones of the bond region.

1. Introduction

In recent years, the transient liquid phase bonding (TLPB) process has been widely studied [1,2] in order to improve the characteristics of the joints by means of composition and microstructure homogenization along the joined pieces.

TLPB process is commonly used in the aerospace industry - mainly superalloys [1], and involves three main steps, namely, liquefaction of the interlayer and base metal (BM) dissolution, liquid phase isothermal solidification and solute homogenization – with and without applied pressure [1,3,4].

On the other hand, is one of the technologies selected to overcome the known problems involved in threaded and coupled connection for oil country tubular goods (OCTG), particularly hot-rolled seamless steel tubes. TLPB of carbon hot-rolled seamless steel tubes, with Fe-based and Ni-based amorphous interlayers and under different conditions, were performed [5–7]. But only their measured mechanical properties were informed, giving no insight about the obtained microstructures.

In a previous work [8], an extensive microstructural characterization of TLPB of low carbon cold-drawn seamless steel tubes, using an amorphous $Fe_{96.2}B_{3.8}$ (in wt%) foil as interlayer, were carried out under different holding times for the isothermal solidification stage and applied pressures. It was observed that increasing pressures reduced the isothermal solidification stage time. This is due to liquid ejection from the joint as well as increased contact of abutting surfaces. On the other hand, the scarce availability of amorphous Fe–B foils prevents its industrial application.

In this study, TLPB was performed to join low carbon hot-rolled seamless steel tubes using as interlayer a commercial amorphous foil of the Fe–Si–B system. A thorough microstructure and mechanical characterization of the joint region (JR) was done and compared with that of the BM to evaluate the applicability of TLPB to OCTG tubular products.

* Corresponding author at: Laboratoire des Matériaux et du Génie Physique (CNRS UMR 5628), Grenoble Institute of Technology, MINATEC, Grenoble Cedex 1, France. Tel.: +33 0456529328.
E-mail address: nicolasdiluozzo@gmail.com (N. Di Luozzo).

0925-8388/$ - see front matter © 2013 Elsevier B.V. All rights reserved.
http://dx.doi.org/10.1016/j.jallcom.2013.11.161

2. Experimental

2.1. Transient liquid phase bonding process

The materials used in this study are hot-rolled carbon seamless steel tubes EN 10297-1 Grade E235, as BM, and amorphous METGLAS® SA1 foil, as interlayer. Their chemical compositions are listed in Table 1. The steel tubes have an outside diameter of 73 mm and a wall thickness of 9.5 mm. The interlayer has a thickness of 25 μm.

The tubes are aligned with their butted surfaces in contact with the interlayer. The butted surfaces had a roughness average (Ra) of 10.8 μm on an evaluation length of 7.5 mm with a cut-off length of 2.5 mm. The joint was placed into the coil of an induction furnace under a controlled reducing (10% H_2 + 90% Ar) atmosphere. The temperature was measured at the joint on the outer surface of the tube by means of infrared thermometry, at a sensing wavelength of 1600 nm. It was raised to the process temperature TP (≈1300 °C), held constant for 7 min, and then cooled in still air to room temperature. A uniaxial pressure of 5 MPa was applied during the bonding process.

2.2. Microstructure characterization

The samples for the microstructural characterization were cut perpendicularly to the joint, that is, along the rolling direction of the tubes.

Electron backscatter diffraction (EBSD) was used to obtain inverse pole figure (IPF) maps. Measurements were done in Zeiss Ultra 55 field-emission gun-scanning electron microscope (FEG-SEM), equipped with an EBSD detector EDAX DigiView III. The data was post-processed by means of EDAX OIM Analysis software. Step sizes of 1 and 2 μm were used for scanning, with an acceleration voltage of 20 kV.

Microstructure characterization was carried out with FEI Quanta 250 FEG-SEM, using an acceleration voltage of 15 kV.

Chemical analysis was performed by electron probe microanalysis (EPMA) with CAMECA SX50.

The samples preparation was carried out using mechanical polishing. It was performed according to the following procedures: after surface grinding, specimens were polished with diamond suspension of 6 and 1 μm. The final polishing varies in each analysis: 0.05 μm colloidal silica suspension for EBSD, 0.3 μm alumina suspension followed by etching with 2% Nital solution for 30 s for FEG-SEM, and no final polishing nor etching for EPMA.

2.3. Mechanical properties characterization

The mechanical properties of the JR and the BM were evaluated by tensile and hardness tests.

Table 1
Chemical composition for E235 steel and SA1 interlayer (in wt%).

	C	Mn	Si	S	P	B	Fe
E235	0.12	1.09	0.24	0.0012	0.015	–	Balance
SA1			5			3	Balance

The tensile samples were cut both from the joined tubes and a tube in the as-received condition in accordance to ASTM E8 M (5 mm thickness, 120 mm gauge length and 13 mm gauge width). The tensile tests were performed at a strain rate of 8 mm/min.

Microindentation hardness profiles across the bonding zone were carried out using a 200 gf load at the JR and a 1000 gf load at the heat affected zone (HAZ) and BM.

3. Results and discussion

3.1. Microstructural characterization

Microstructure of the BM and the HAZ

The BM contained ferrite and pearlite with a prominent banded structure as shown in Fig. 1(a). From EBSD analysis of the microstructure we obtained:

- An average grain diameter of 19 μm.
- A misorientation angle distribution plot (Fig. 1(b)) close to a randomly oriented assembly of grains, with a small shift towards lower misorientations.
- From grain boundary character distribution analysis – where boundaries with angles $\theta \leqslant 15°$ are classified as low-angle grain boundaries (LAGBs) whereas boundaries with $\theta > 15°$ are denoted as high-angle grain boundaries (HAGB) – we obtained that HAGB fraction (69.7%) is much larger than LAGB fraction (15.6%) and coincident site lattice (CSL) (14.7%).

From above it can be concluded that the BM microstructure is almost fully recrystallized [9]. This is intrinsic of hot-rolling process, which has a phase transformation after plastic deformation. The texture generated during hot-rolling is mostly destroyed by the subsequent phase transformation from austenite to ferrite.

The HAZ also contained ferrite and pearlite, but the banded structure was removed (Fig. 2(a)). From EBSD analysis of the microstructure we obtained:

- An average grain diameter of 47 μm.
- A misorientation angle distribution plot (Fig. 2(b)) which shifts markedly towards lower misorientations.
- From grain boundary character distribution analysis we obtained that LAGB fraction clearly increased (40.4%), at the expense of HAGB (50.0%) and CSL (9.6%).

We can conclude that HAZ meets all requirements of a recrystallized microstructure that suffered a grain growth process [10].

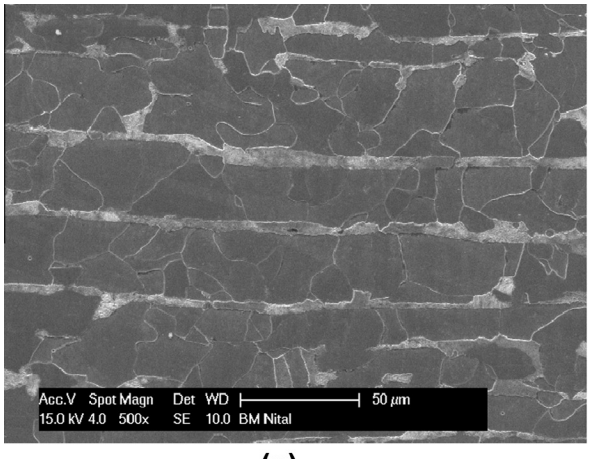

(a)

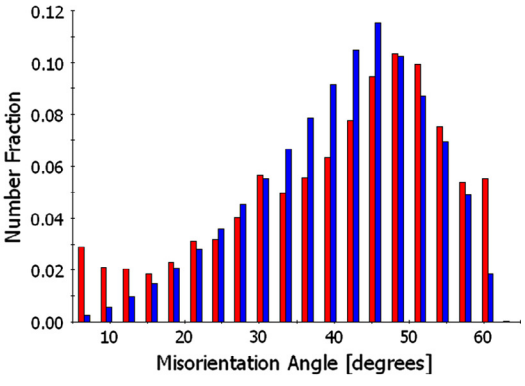

(b)

Fig. 1. (a) Microstructure of the BM: FEG-SEM micrograph showing ferrite/pearlite bands – nital etched (b) Misorientation angle distribution plots of the BM (red) and for a randomly oriented assembly of grains (blue). (For interpretation of the references to colour in this figure legend, the reader is referred to the web version of this article.)

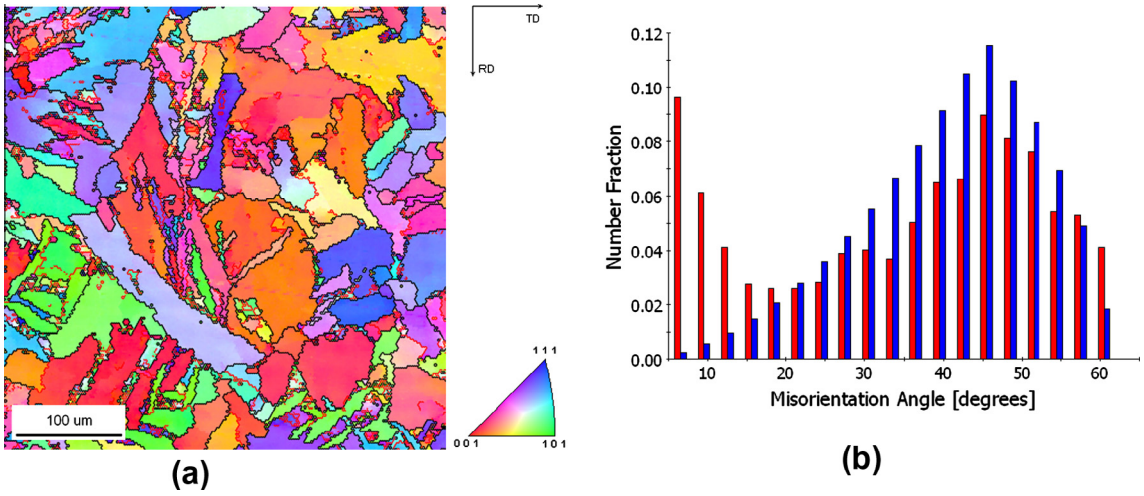

Fig. 2. (a) Microstructure of the HAZ: Normal direction (ND)-projected IPF map –black lines denote HAGB and red lines denote LAGB. The rolling direction (RD) and the transverse direction (TD) are indicated on the figure (b) Grain size distribution plots of the HAZ (red) and for a randomly oriented assembly of grains (blue). (For interpretation of the references to colour in this figure legend, the reader is referred to the web version of this article.)

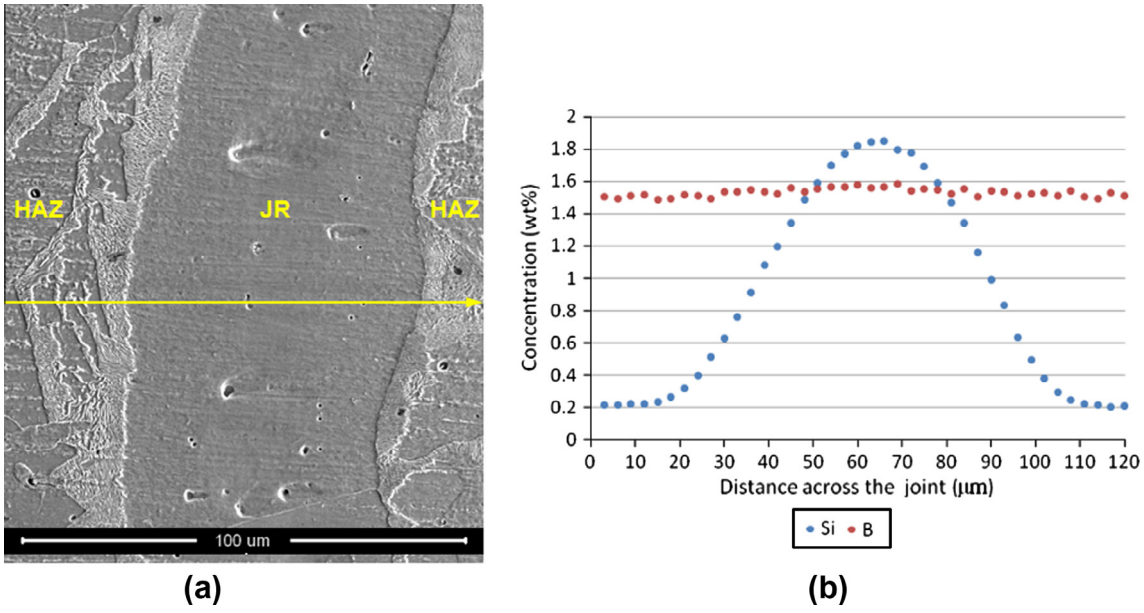

Fig. 3. (a) FEG-SEM micrograph of the joint – secondary electrons. The JR and HAZ are indicated on the figure (b) Concentration profile (by EPMA) of Si and B as indicated in (a) – in yellow. (For interpretation of the references to colour in this figure legend, the reader is referred to the web version of this article.)

Microstructure of the JR

The completion of the solidification process was achieved in the entire JR – that is, the zone in which the microstructure was affected by the different stages of the TLPB process, but does not correspond to the microstructure of the HAZ. Its microstructure consist only of ferrite grains, having a width of ≈70 μm, as shown in Fig. 3(a).

In this region, high Si concentrations are encountered. This explains the absence of cementite, since Si prevents its formation [11]. With respect with B concentration, it has an almost constant profile, having diffused well into the HAZ (Fig. 3(b)).

The interface between the HAZ and the JR, is characterized mostly by grain boundaries, particularly HAGB (Fig. 4). A similar situation was reported in TLPB of commercially pure Ni (as BM) and Ni–Cr–Fe–B–Si amorphous foil (as interlayer) [12], where both borides and grain boundaries acts as an interface between the previous liquid phase and the HAZ, that is, a non-epitaxial solidification was observed.

In addition with the differences in microstructure, HAGB between the JR and the HAZ are delimiting most of the extent of the dissolution stage, namely, the transient liquid phase zone, and are indicating that the grains at the JR were able to solidify non-epitaxially from those of the HAZ.

It is worth noting that the fact that the JR is almost three times wider compared with the interlayer is connected with the dissolution of the BM [3], just before isothermal solidification. Similar observations can be found in [12]. During this stage, B and Si from the interlayer - now liquid - begin to diffuse into the BM resulting in an impoverishment of these elements at the transient liquid phase. On the other hand, B and Si act as melting point depressants for the steel, and each volume of steel whose melting point reaches TP, is melted, widening the liquid gap. The above mentioned stage

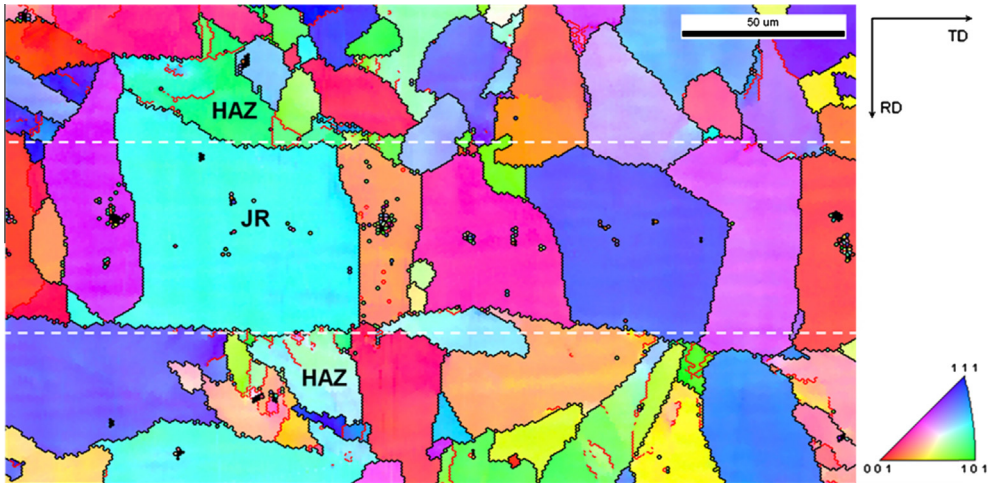

Fig. 4. ND-projected IPF map from the JR. In the map, black lines denote HAGB and red lines denote LAGB. The JR and HAZ are indicated on the figure. The white dotted lines are a guide to the eye of the extension of the JR. (For interpretation of the references to colour in this figure legend, the reader is referred to the web version of this article.)

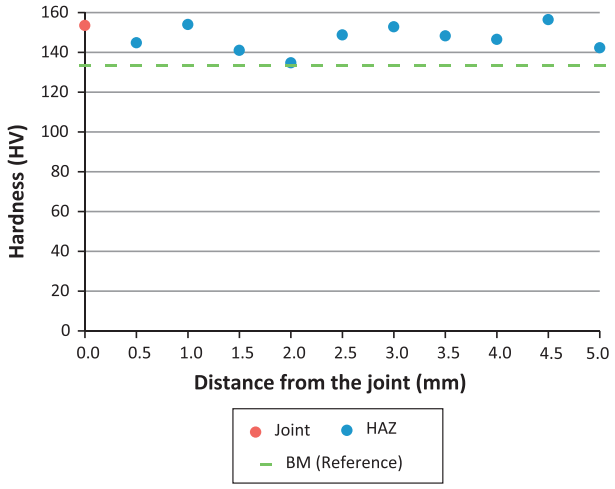

Fig. 5. Hardness distribution across the bonding zone.

of the process is directly connected with the measured chemical composition profiles at the JR, which are very different from that of the interlayer.

3.2. Mechanical properties

Tensile test

The tensile test of the bonded sample gave an ultimate tensile stress (UTS) of 490 MPa - achieving 96% of the UTS of the BM in the as-received condition - 512 MPa, with failure occurring well away from the JR.

The small reduction of the UTS, compared with the BM, can be due to the deleterious effects of the TLPB thermal cycle, mainly the removal of the banded structure and grain growth.

Hardness profiles

Microindentation testing was carried out to display the hardness values at different zones in the bonded part. The hardness profile is shown in Fig. 5. After bonding process, the hardness both at the JR and at the HAZ next to the JR is slightly higher than that of the BM. This can be explained as follows:

- The JR is enriched in Si, which is usually used to increase hardness [13].
- The cementite fraction at the HAZ next to the JR is slightly higher than that of the BM, leading to an increase in hardness. This is due to the fact that this zone was cooled to room temperature more rapidly than the whole tube after the hot-rolling process.

4. Conclusions

The TLBP process was successfully used to join low carbon hot-rolled seamless steel tubes using an amorphous Fe–B–Si foil as interlayer.

It was observed that at the HAZ, the almost fully recrystallized banded microstructure of the BM changed to one subjected to grain growth, with complete removal of the ferrite/pearlite bands.

The completion of the solidification process was achieved in the entire JR. The microstructure consists only of ferrite grains. High Si concentrations are encountered, while B concentrations are almost constant, having diffused well into the HAZ. Finally, the interface between the HAZ and the ferrite grains at the JR is composed mostly by HAGB. We can conclude that these HAGB are delimiting most of the extent of the dissolution stage, that is, the transient liquid phase zone, and that the crystal orientations of the isothermally solidified grains at the JR are generally different from those of the HAZ, indicating that the solidification process was carried out in non-epitaxial conditions. As well, an extensive dissolution of the BM is observed compared with the thickness of the interlayer.

On the other hand, the mechanical characterization showed that the JR has more strength than the HAZ when tensile tested - the failure occurs away from the JR - and the hardness of the JR was above the BM measured values.

With the above mentioned, we can conclude that TLPB can be suitable to a variety of tubular products for the OCTG industry.

Acknowledgements

Financial support from the European Commission (Arcoiris Erasmus Mundus Scholarship) and from the FIUBA is gratefully acknowledged.

References

[1] S. Duvall, W.A. Owczarski, D.F. Paulonis, Weld. J. 204 (1974) 203–214.
[2] W.D. MacDonald, T.W. Eagar, Metall. Trans. A 29 (1988) 315–325, http://dx.doi.org/10.1007/s11661-998-0183-1.
[3] I. Tuah-Poku, M. Dollar, T.B. Massalski, Metall. Trans. A 19 (1988) 675–686, http://dx.doi.org/10.1007/BF02649282.
[4] W.F. Gale, D.A. Butts, Sci. Technol. Weld. Joining 9 (2004) 283–300, http://dx.doi.org/10.1179/136217104225021724.
[5] S. Kishi, T. Maenosono, M. Sato, US Patent 5875954, 1999.
[6] Y. Hamada, Y. Fukada, M. Ueda, Y. Komizo, US Patent 6059175, 2000.
[7] T. Shimizu, H. Horio, K. Kito, S. Inagaki, R. Yamada, US Patent 6592154 B2, 2003.
[8] N. Di Luozzo, M. Fontana, B. Arcondo, J. Mater. Sci. 43 (2008) 4938–4944, http://dx.doi.org/10.1007/s10853-008-2720-0.
[9] R. Saha, R.K. Ray, Mater. Sci. Eng. A 527 (2010) 1882–1890, http://dx.doi.org/10.1016/j.msea.2009.11.019.
[10] F.J. Humphreys, M. Hatherly, Recrystallization and Related Annealing Phenomena, Elsevier, Amsterdam, 2004.
[11] H. Bhadeshia, R. Honeycombe, Steels: Microstructure and Properties, Elsevier, Amsterdam, 2006.
[12] J. Ruiz-Vargas, N. Siredey-Schwaller, N. Gey, P. Bocher, A. Hazotte, J. Mater. Process. Technol. 213 (2013) 20–29, http://dx.doi.org/10.1016/j.jmatprotec.2012.07.016.
[13] B.L. Bramfitt, A.O. Benscoter, Metallographer's Guide: Practices and Procedures for Irons and Steels, ASM International, Novelty, 2002.